Light irradiation controlled spin selectivity in a magnetic helix

Moumita Dey,[1] Suparna Sarkar,[2] and Santanu K. Maiti[2,*]

[1]*Department of Physics, Adamas University, Adamas Knowledge City, Barasat-Barrackpore Road, 24 Parganas North, Kolkata-700 126, India*

[2]*Physics and Applied Mathematics Unit, Indian Statistical Institute, 203 Barrackpore Trunk Road, Kolkata-700 108, India*

(Received 2 August 2023; revised 24 September 2023; accepted 25 September 2023; published 9 October 2023)

The present work critically investigates the interplay between light irradiation, molecular helicity, and electron hopping on spin-selective electron transmission, considering a magnetic helix as the functional element. Depending on the range of electron hopping, short-range and long-range ones, two different kinds of magnetic helices are taken into account. The common examples of these two different ranges of electron hopping are single-stranded DNA and protein molecules respectively. Each magnetic helix is subjected to a circularly polarized light which is applied perpendicular to the helix axis. The transmission spectra associated with up and down spin electrons get significantly modified, resulting in a high degree of spin polarization even when the Fermi energy is placed near the band center. The performance becomes superior with increasing the range of electron hopping. A tight-binding framework is given to describe the system, where the effect of light is incorporated through the minimal coupling approach following the Floquet-Bloch ansatz. All the results are worked out based on the standard Green's function formalism. The degree of spin polarization and its phase can be monitored selectively by means of light. To strengthen the impact of helicity, a comparative study is also made considering twist-free geometry and other twisted magnetic systems. Finally, a brief outline of the possible routes of designing magnetic helices is given, for the sake of completeness of work. Our analysis may provide some insights to achieve controlled spin-based electronic devices using different types of light-driven magnetic helices that are described beyond the conventional nearest-neighbor hopping model.

DOI: 10.1103/PhysRevB.108.155408

I. INTRODUCTION

Over a long period of time, ferromagnetic (FM) materials have been actively used for studying spin-dependent transport phenomena [1–3]. Though there exist some unavoidable limitations, like resistivity mismatch in contact interfaces and regulation of electron spin by confining a magnetic field in a small-scale region, such systems can always give a large mismatch between up and down spin energy channels due to high spin-dependent scattering strength [4], compared to other spin-dependent scattering mechanisms [5–10].

For a purposeful design of spin-based electronic devices, the separation of up and down spin electrons, more precisely, we can say, the generation of polarized spin current from an unpolarized electron beam is one of the prime requirements [11–14]. The researchers in this field have essentially paid attention to this issue, and over the last several years, no doubt a wealth of literature knowledge has already been established [12,15–19]. However, the fact is that most of the studies, especially theoretical ones, associated with spin filtration are involved with linear shape geometries be they one-dimensional or higher, and very little effort has been given considering geometrical twisting. The latter type of system has been triggered following the pioneering work of Gohler *et al.* [20], where they have shown that chiral molecules can have the capacity to produce a high degree of spin filtration due to their unique and diverse characteristic features. In their experimental work, it has been established that more than 60% spin polarization (SP) can be achieved even for the limit of room temperature. They considered self-assembled monolayers of double-stranded DNA (ds-DNA) molecules and deposited them on a gold substrate. When the substrate is irradiated with light, it emits photoelectrons. Both up and down spin electrons are generated from the substrate but when they pass through the molecular system, one of the spin components is highly screened, depending on the chirality of the molecule, i.e., whether the molecule is right-handed or left-handed. This phenomenon is referred to as *chiral induced spin selectivity* (CISS) [21–27]. Soon after this experiment, several groups have started doing work on spin selectivity using different kinds of helical molecules as well as tailor-made helical systems, to understand the basic mechanisms of getting a high degree of spin filtration [28–33].

Most of the available works using helical systems have concentrated on spin-orbit (SO) coupling as the spin-dependent scattering factor [31–35]. The SO coupling has of course some additional advantages [36–41] compared to the other sources of spin-dependent scattering, as the previous one can be tuned at some level with the help of suitable external electrodes placed in the vicinity of the sample. However, there exist some important limitations. It has been checked that the strength of SO coupling is too weak [42], especially for the helical molecular systems (like DNA, protein, etc.), and thus the misalignment of two different spin channels does not occur appreciably which hinders a high degree of spin

*santanu.maiti@isical.ac.in

filtration even for moderate bias voltages. The other important limitation is that, to have ordinary CISS effect we need to impose "dephasing" into the system [31], as without dephasing time-reversal symmetry is not broken and then spin polarization cannot be observed. However, dephasing, on the other hand, strongly disrupts the phenomenon of quantum interference which therefore reduces the response. So, elimination of dephasing was a long standing story. Very recently Phuc has explicitly shown that [43,44] CISS effect can be observed in 'achiral' molecules and materials, driven by an externally circularly polarized laser field, and here dephasing mechanism is absolutely not required. The light-matter interaction effectively breaks the time-reversal symmetry which leads to finite spin-dependent transport. This is referred to as Floquet-engineered CISS in achiral matters and the prescription is quite different than the ordinary CISS as observed in chiral molecules. In Phuc's prescription, the one important restriction is that high degree of spin polarization in achiral molecules can be obtained when the average chemical potential of the two baths lies with a too narrow range due to high frequency laser field. A broader energy range might be expected by combining chiral molecules with light-matter interaction, as noted by Phuc, but since in these cases, SO coupling is the spin-dependent scattering factor, it will be quite hard to get a high degree of spin polarization for a reasonable bias window.

All the above facts have triggered us to find any other alternative prescription where on one hand we can circumvent the use of SO coupling and on the other hand we can achieve Floquet-engineered CISS effect. To do that, in the present work, we choose a helical magnetic system, which is referred to as *ferromagnetic helix*, and we apply a circularly polarized light perpendicular to the helix axis (see Fig. 1) that essentially controls the transport behavior. For our helical system, we can have two different ranges of electron hopping upon setting the physical parameters. In one case we get a short-range hopping (SRH) helix and in the other case a long-range hopping (LRH) helix [32]. The most common and realistic examples where we can have short-range and long-range hoppings of electrons are DNA and protein molecules [32,33], respectively, and nowadays with the help of sophisticated experimental facilities different kinds of such helical systems are fabricated (a brief discussion about the possibilities of designing helical systems is available at the end of our analysis). *The central focus of our work is to inspect the interplay between helicity, light irradiation, and different ranges of electron hopping on spin filtration, which might be an interesting observation.* Our proposition may provide some important inputs to achieve selective spin transfer by means of light irradiation through different types of magnetic helices those are described beyond the usual nearest-neighbor electron hopping.

Here it is relevant to point out that in our earlier work [28], we have studied spin-filtration in magnetic helices in presence of a transverse electric field. That kind of field can be produced with the help of suitable gate electrodes placing near the vicinity of the helical system. An elaborate discussion of it is given in Ref. [45], and we have followed that. In the presence of the perpendicular electric field, the site energies get modified in a cosine form (see Eq. (2) of Ref. [28]) which makes the system a 'correlated' disordered one. As the system becomes more disordered with increasing the field strength, we always need to restrict ourselves in the weak disordered regime, otherwise all the energy eigenstates will be localized and no spin dependent phenomena will be observed. In contrast to it, our proposed driven magnetic helix in the present work is not a disordered one, rather the hopping integrals get renormalized as per the Floquet-Bloch (FB) ansatz [46,47] and more suitable control of spin transfer can be made in a wide range of bias window.

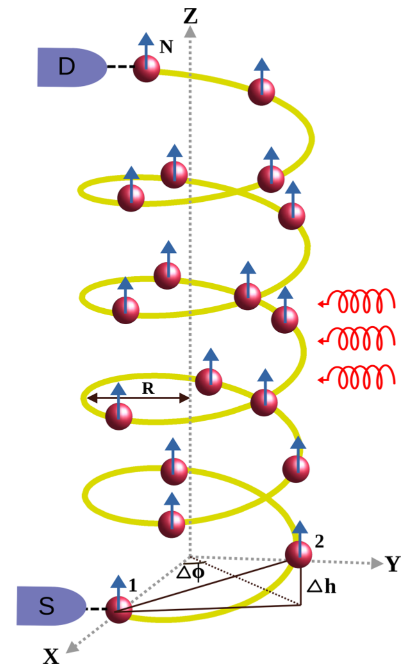

FIG. 1. Spin polarized junction setup where a right-handed ferromagnetic helix is clamped between source and drain electrodes. A circularly polarized light (red spiral curves) is applied perpendicular to the helix axis that selectively controls the spin-dependent electron transmission.

To study transport phenomena through driven magnetic helix, two contact electrodes, namely source (S) and drain (D) are coupled to two end lattice sites of the helix (Fig. 1). The full junction setup is described within a tight-binding (TB) framework that always gives a simple level of description. The light irradiation is included in the Hamiltonian through a minimal coupling scheme following the FB theory [46,47]. All the results are worked out based on the standard Green's function formalism [48–51]. The important findings of our work are: (i) achieving a high degree of spin filtration coefficient by means of light and that is even possible when the Fermi energy is placed very near to the band center, (ii) complete phase reversal of spin polarization (100% up to down spin polarization and vice versa) by tuning light, and (iii) all the results are valid for a broad range of physical parameters. The present analysis may lead to a possible route for designing efficient spin-based electronic devices using irradiated magnetic helices, and can be extended further for similar kinds of other helical magnetic systems as well.

The rest part of the paper is arranged as follows. Section II contains the description of the physical setup for spin filtration, tight-binding Hamiltonian, and the theoretical framework for calculating the numerical results. In Appendix A, a detailed derivation for calculating effective hopping strength in presence of light irradiation following the FB method is given, for the benefit of the readers. All the essential results of SRH and LRH systems are presented and thoroughly discussed in Sec. III. At the end of Sec. III, a brief outline of experimental possibilities for achieving magnetic helices is given. In Appendix B, a basic result is given for the conventional nearest-neighbor hopping (NNH) model to compare with the systems that are described beyond NNH. The key findings of the work are summarized in Sec. IV.

II. QUANTUM SYSTEM, TIGHT-BINDING HAMILTONIAN AND THEORETICAL FORMALISM

A. Spin polarized setup and the TB Hamiltonian

The schematic diagram of the functional element, i.e., the magnetic helix system is shown in Fig. 1. The helix is comprised of N lattice sites, where each site contains a finite magnetic moment (shown by the blue arrow). Any specific orientation of these moments can be taken into account, and the general orientation is described by usual polar angle θ_i and azimuthal angle φ_i (i being the lattice site index), in spherical polar coordinate system. In our analysis, we assume that all the magnetic moments are identical and they are aligned along $+Z$ direction (chosen spin quantized direction of our analysis), without loss of generality.

Two most important physical parameters associated with the helix system are (i) twisting angle $\Delta\phi$ and (ii) stacking distance Δh. The twisting angle measures how one atomic site is twisted with respect to the other and the stacking distance describes how close the neighboring sites are stacked. Usually when Δh is reasonably small, i.e., the atoms are closely packed, electrons can easily hop from one site to all other available sites of the helix, making the system a long-range one. While for the other case, where the stacking distance is quite large, electrons can hop to the few neighboring sites, yielding the helix a short-range one. In our work, we concentrate on both these helices to have a clear understanding of the role of electron hopping on spin dependent transport phenomena. The other physical parameter R is also associated with the helix that measures the radius of the circle when the helix is projected in the X-Y plane. A circularly polarized light is injected perpendicular to the helix axis, which plays the central role of our analysis.

In order to study transport phenomena we need to couple the magnetic helix with two contact electrodes. The electrodes are refereed to as source (S) and drain (D), and they are attached to the two end magnetic sites of the helix. The electrodes are assumed to be nonmagnetic and one-dimensional.

The spin-polarized setup is simulated by a tight-binding Hamiltonian. First we consider the situation where light is not applied to the helix. Its inclusion into the Hamiltonian is described in the subsequent part, as it is quite lengthy. The Hamiltonian of the full system, i.e., source-helix-drain nanojunction can be written as

$$\mathcal{H} = \mathcal{H}_{\text{FM}} + \mathcal{H}_S + \mathcal{H}_D + \mathcal{H}_{\text{cl}}, \tag{1}$$

where different terms in the right hand side are associated with different parts of the nanojunction, and they are explicitly described as follows. The first term $\mathcal{H}_{\text{FM}}$ corresponds to the sub-Hamiltonian of the FM helix, and its general form looks like (applicable both for SRH and LRH helices)

$$\mathcal{H}_{\text{FM}} = \sum_{n=1}^{N} \boldsymbol{c}_n^\dagger(\boldsymbol{\epsilon}_n - \vec{\mathfrak{h}}_n\cdot\vec{\sigma})\boldsymbol{c}_n + \sum_{n=1}^{N-1}\sum_{j=1}^{N-n}(\boldsymbol{c}_n^\dagger \boldsymbol{t}_{nj}\boldsymbol{c}_{n+j} + \text{H.c.}), \tag{2}$$

where $\boldsymbol{c}_n^\dagger = (c_{n\uparrow}^\dagger \quad c_{n\downarrow}^\dagger)$. $c_{n\sigma}^\dagger$ ($c_{n\sigma}$) is the fermionic creation (annihilation) operator of an electron at site i with spin σ ($\uparrow,\downarrow$). $(\boldsymbol{\epsilon}_n - \vec{\mathfrak{h}}_n\cdot\vec{\sigma})$ is the effective site energy matrix, having dimension (2×2), where $\boldsymbol{\epsilon}_n = \text{diag}(\epsilon_{n\uparrow},\epsilon_{n\downarrow})$. $\epsilon_{n\sigma}$ is the site energy in the absence of spin-moment scattering. $\vec{\mathfrak{h}}_n\cdot\vec{\sigma}$ is responsible for scattering, where $\vec{\sigma}$ is the Pauli spin vector and $\vec{\mathfrak{h}}_n$ is the spin dependent scattering factor. When an itinerant electron interacts with a local magnetic moment then the scattering takes place. More explicitly, we can write the term $\vec{\mathfrak{h}}_{\text{n}}\cdot\vec{\sigma}$ as $J\langle\vec{S}_n\rangle\cdot\vec{\sigma}$, where $\langle\vec{S}_n\rangle$ is the net spin at site n and J is the coupling strength. $\boldsymbol{t}_{nj} = \text{diag}(t_{nj}, t_{nj})$, where t_{nj} corresponds to the electron hopping between the sites n and $(n+j)$ of the magnetic helix.

The hopping integral t_{nj} is written in the form [33]

$$t_{nj} = t_1 e^{-(l_{nj}-l_1)/l_c} \tag{3}$$

where t_1 is the nearest-neighbor hopping strength. The parameter l_{nj} measures the distance between site n and $(n+j)$ and l_1 denotes the nearest-neighbor distance. l_c is the decay constant. In terms of the twisting angle $\Delta\phi$, stacking distance Δh and radius R, l_{nj} is expressed as [33]

$$l_{nj} = \sqrt{4R^2\sin^2(j\Delta\phi/2) + (j\Delta h)^2}. \tag{4}$$

(1) *Inclusion of light irradiation*. A uniform light is applied along the perpendicular direction of the magnetic helix (red spiral curves in Fig. 1). A minimal coupling scheme following the Floquet-Bloch ansatz is used to incorporate the effect of irradiation [46,47]. In our analysis, we assume a circularly polarized light, and since the incident direction is along Y axis, the vector potential $\vec{A}(\tau)$ that summarizes the irradiation can be expresses as

$$\vec{A}(\tau) = A_0\cos\omega\tau\,\hat{i} + A_0\sin\omega\tau\,\hat{k}, \tag{5}$$

where A_0 is the amplitude, ω is the frequency, and τ is the time.

Due to irradiation, the hopping strength gets modified as (complete derivation is provided in Appendix A)

$$\tilde{t}_{nj}^{p,q} = t_{nj}\frac{1}{\mathcal{T}}\int_0^{\mathcal{T}} e^{-i\omega\tau(p-q)}e^{i\vec{A}\cdot(\vec{R}_{nj}-\vec{R}_n)}d\tau\, e^{-(l_{nj}-l_1)/l_c}, \tag{6}$$

where $\mathcal{T}(=2\pi/\omega)$ is the time period of the incident irradiation, $\vec{R}_{nj}$ and $\vec{R}_n$ are the radius vectors of $(n+j)$th and nth sites, respectively, and p and q (integers) are associated with the Floquet bands.

Calculation of $(\vec{R}_{nj}-\vec{R}_n)$. To calculate the distance between nth and $(n+j)$th sites, we start with component wise evaluation. We assume that the first site of the magnetic helix is placed on the X axis. Thus the X, Y, and Z components of the nth site can be written as

$$X_n = R\cos\{(n-1)\Delta\phi\},$$
$$Y_n = R\sin\{(n-1)\Delta\phi\},$$
$$Z_n = (n-1)\Delta h.$$

Similarly, for $(n+j)$th site, the components are

$$X_{n+j} = R\cos\{(n+j-1)\Delta\phi\},$$
$$Y_{n+j} = R\sin\{(n+j-1)\Delta\phi\},$$
$$Z_{n+j} = (n+j-1)\Delta h.$$

Therefore the X, Y, and Z components of the radius vector $(\vec{R}_{nj} - \vec{R}_n)$ are given by

$$\begin{aligned} a_x^{nj} &= X_{n+j} - X_n \\ &= -2R\sin\left(n\Delta\phi - \Delta\phi + \frac{j\Delta\phi}{2}\right)\sin\left(\frac{j\Delta\phi}{2}\right), \\ a_y^{nj} &= Y_{n+j} - Y_n \\ &= 2R\sin\left(n\Delta\phi - \Delta\phi + \frac{j\Delta\phi}{2}\right)\sin\left(\frac{j\Delta\phi}{2}\right), \end{aligned}$$

and

$$a_z^{nj} = Z_{n+j} - Z_n = j\Delta h.$$

Thus $\vec{R}_{nj} - \vec{R}_n = a_x^{nj}\,\hat{i} + a_y^{nj}\,\hat{j} + a_z^{nj}\,\hat{k}$, where $\hat{i}$, $\hat{j}$, and $\hat{k}$ are the unit vectors along X, Y, and Z directions, respectively.

We assume that the light is applied along the Y direction. Now due to the geometry of the magnetic helix, the incidence angle of the light changes along the circumference, and hence the effective magnetic vector potential can be written as

$$\begin{aligned} \vec{A}_{\text{eff}} &= \boldsymbol{R}_Z(\Delta\phi)\vec{A} \\ &= \begin{pmatrix} \cos\Delta\phi & \sin\Delta\phi & 0 \\ -\sin\Delta\phi & \cos\Delta\phi & 0 \\ 0 & 0 & 1 \end{pmatrix} \begin{pmatrix} A_x \\ 0 \\ A_z \end{pmatrix} \\ &= A_x\cos\Delta\phi\,\hat{i} - A_x\sin\Delta\phi\,\hat{j} + A_z\,\hat{k}. \end{aligned}$$

Using this effective vector potential and substituting the components of $(\vec{R}_{nj} - \vec{R}_n)$, we calculate the factor $\vec{A}.(\vec{R}_{nj} - \vec{R}_n)$ which simplifies to

$$\vec{A}.(\vec{R}_{nj} - \vec{R}_n) = \Lambda\sin(\omega\tau + \psi),$$

where

$$\Lambda = A_0\sqrt{\left(a_z^{nj}\right)^2 + \left(a_x^{nj}\right)^2\cos^2\Delta\phi + \left(a_y^{nj}\right)^2\sin^2\Delta\phi - \left(a_x^{nj}\right)\left(a_y^{nj}\right)\sin(2\Delta\phi)}$$

and

$$\psi = \tan^{-1}\left(\frac{a_x^{nj}\cos\Delta\phi - a_y^{nj}\sin\Delta\phi}{a_z^{nj}}\right). \tag{7}$$

Plugging this term in Eq. (6) and doing some algebra, we get

$$\tilde{t}_{nj}^{p,q} = t_{nj}J_{p-q}(\Lambda)e^{i\Theta}e^{-(l_{nj}-l_1)/l_c},$$

where $\Theta = (p-q)\tan^{-1}(\frac{a_x^{nj}\cos\Delta\phi - a_y^{nj}\sin\Delta\phi}{a_z^{nj}})$ and $J_{p-q}(\Lambda)$ corresponds to the $(p-q)$th order Bessel function of first kind. Thus, in the presence of irradiation, the hopping integrals get changed, and accordingly, it is expected that the spin-dependent transport phenomena will be modified.

Additional note. Here, it is important to emphasize that in our current research, we exclusively focus on periodically driven quantum systems for the sake of simplicity. For such systems, the Floquet-based approach mentioned earlier is highly applicable. However, the fact is that, Floquet theory has some important limitations, particularly when we think about the systems beyond periodic driving [52–54]. In their study [52], Stefanucci *et al.* have shown that for nonperiodic driving cases, Floquet formalism does not work, and they have provided an alternative prescription that can safely be used for different nonperiodic driving systems. Moreover the computation cost is also not so heavy. We will try to extend our study in presence of any arbitrary driving field in our forthcoming work. For time-dependent transport, several other methodologies have also been given by Stefanucci and coworkers, and for the details see Refs. [55–57].

The sub-Hamiltonians $\mathcal{H}_S$ and $\mathcal{H}_D$ are associated with the source and drain electrodes. They are expressed in a simple form (since magnetic interaction is not there and only NNH is taken into account) as

$$\mathcal{H}_S = \mathcal{H}_D = \sum_i \boldsymbol{a}_i^\dagger \boldsymbol{\epsilon}_0 \boldsymbol{a}_i + \sum_i (\boldsymbol{a}_{i+1}^\dagger \boldsymbol{t}_0 \boldsymbol{a}_i + \text{H.c.}), \tag{8}$$

where $\boldsymbol{a}_i^\dagger = (a_{i\uparrow}^\dagger \quad a_{i\downarrow}^\dagger)$, $\boldsymbol{\epsilon}_0 = \text{diag}(\epsilon_0, \epsilon_0)$, and $\boldsymbol{t}_0 = \text{diag}(t_0, t_0)$. ϵ_0 and t_0 are the site energy and NNH integral, respectively.

These electrodes are coupled to the sites 1 and N of the magnetic helix. If τ_S and τ_D are the coupling strengths of the helix with S and D respectively then the coupling Hamiltonian reads as

$$\mathcal{H}_{\text{cl}} = \boldsymbol{c}_1^\dagger \boldsymbol{\tau}_S \boldsymbol{a}_{-1} + \boldsymbol{c}_N^\dagger \boldsymbol{\tau}_D \boldsymbol{a}_{N+1} + \text{H.c.}, \tag{9}$$

where $\boldsymbol{\tau}_S = \text{diag}(\tau_S, \tau_S)$ and $\boldsymbol{\tau}_D = \text{diag}(\tau_D, \tau_D)$.

B. Theoretical formalism: Green's function technique

To study spin-dependent transport phenomena and to determine the degree of spin polarization, first we need to calculate spin-specific transmission probabilities, and for that, we use Green's function (GF) technique [48–51]. This technique is the most standard one compared to the other available approaches like transfer-matrix and wave-guide methods. The classic advantage is that, in GF approach, the effects of contact electrodes can easily be incorporated to the functional element that is clamped between them, via the self-energy correction. For a detailed calculation of self-energies due to contact electrodes, see Refs. [48,49], and the references therein.

Two Green's functions $\boldsymbol{G}^r$ and $\boldsymbol{G}^a$, referred to as retarded and advanced Green's functions respectively, are used in order to find transmission coefficients and they are expressed as [48,49]

$$\boldsymbol{G}^r = (\boldsymbol{G}^a)^\dagger = [E\boldsymbol{I} - \mathcal{H}_{\text{FM}} - \boldsymbol{\Sigma}_S - \boldsymbol{\Sigma}_D]^{-1},$$

where E is the energy and $\boldsymbol{I}$ represents the identity matrix having the dimension $(2N \times 2N)$. N being the total number of lattice sites in the magnetic helix, and the factor 2 arises due to up and down spins. $\boldsymbol{\Sigma}_S$ and $\boldsymbol{\Sigma}_D$ are the contact self-energies for the source and drain, respectively. Using the retarded and advanced Green's functions, spin-dependent transmission probability is determined from the expression [48,51]

$$T_{\sigma\sigma'} = \mathrm{Tr}\big[\boldsymbol{\Gamma}_S^{\sigma}\boldsymbol{G}^r\boldsymbol{\Gamma}_D^{\sigma'}\boldsymbol{G}^a\big], \tag{10}$$

where $\boldsymbol{\Gamma}_{S(D)}^{\sigma(\sigma')}$ is the coupling matrix, and, it is connected to the self-energy as

$$\boldsymbol{\Gamma}_{S(D)}^{\sigma(\sigma')} = -2\mathrm{Im}\big[\boldsymbol{\Sigma}_{S(D)}^{\sigma(\sigma')}\big].$$

The factor $T_{\sigma\sigma'}$ measures the transmission probability of an electron with spin σ' that is injected with spin σ in the magnetic helix. Depending on σ and σ', we have four possible transmission coefficients, among which two are referred to as pure spin transmission ($\sigma = \sigma'$), and the other two represent spin-flip transmission ($\sigma \neq \sigma'$). From the coefficients we eventually determine the net up and down spin transmission probabilities following the relations

$$T_{\uparrow} = T_{\uparrow\uparrow} + T_{\downarrow\uparrow} \text{ and } T_{\downarrow} = T_{\downarrow\downarrow} + T_{\uparrow\downarrow},$$

respectively.

Utilizing the transmission probability function, we compute spin-dependent transport current through the junction following the Landauer-Büttiker prescription. At zero temperature and for a fixed bias voltage V, the spin-specific current is expressed as [48]

$$I_{\sigma} = \left(\frac{e}{h}\right)\int_{E_F-\frac{eV}{2}}^{E_F+\frac{eV}{2}} T_{\sigma}(E)\,dE, \tag{11}$$

where e is the electronic charge, h is the Plank constant, and E_F is the equilibrium Fermi energy. Thus an integration of the transmission function T_{σ} over the energy window $E_F - eV/2 \leqslant E \leqslant E_F + eV/2$ has to be done to find the current.

Finally, we compute spin polarization coefficient through the relation [58,59]

$$P = \frac{I_{\uparrow} - I_{\downarrow}}{I_{\uparrow} + I_{\downarrow}} \times 100\%. \tag{12}$$

When both the spin electrons propagate with identical probability, no spin polarization occurs i.e., $P = 0$. On the other hand, if only up or down spin electrons propagate through the magnetic helix, the polarization becomes maximum (viz., $P = \pm 100\%$). For other cases, we get intermediate values of P.

III. NUMERICAL RESULTS AND DISCUSSION

Our central focus is to discuss the impact of light irradiation on spin-dependent electron transfer through magnetic helix system and hence the spin polarization. We should try to find out under which condition the spin polarization coefficient reaches to the maximum value, and to check whether it persists for a broad range of input parameters or not. Persistence of favorable responses over a broad range of physical parameters is highly important, considering the experimental perspective of theoretical propositions.

TABLE I. TB parameters of SRH and LRH magnetic helices.

Molecule	R (Å)	Δh (Å)	$\Delta\phi$	l_c (Å)
SRH	7	3.4	$\frac{\pi}{5}$	0.9
LRH	2.5	1.5	$\frac{5\pi}{9}$	0.9

Before coming to the results, let us first specify the parameter values those are kept unchanged throughout the calculations. All the energies are measured in units of electron-volt (eV), and the vector potential is expressed in units of $(el_1/c\hbar)$. In the source and drain electrodes, the on-site energy ϵ_0 and NNH integrals t_0 are set at 0 and 2, respectively. The coupling strengths τ_S and τ_D are fixed at 0.75. In the magnetic helix we take $\epsilon_{n\uparrow} = \epsilon_{n\downarrow} = 0$, and the NNH strength $t_1 = 1$. Unless specified, we choose the values of the physical parameters R, Δh, and $\Delta\phi$ for the SRH and LRH systems as mentioned in Table I. These are the most standard parameter values taken for the SRH and LRH systems [60], and have been considered in several other contemporary works. To show the impact of helicity on spin filtration in a more general way, we add a discussion by changing $\Delta\phi$ in a wide range including the situation where $\Delta\phi$ is explicitly zero viz, in the absence of any helicity. In our chosen magnetic systems, we assume that all the magnetic moments are aligned along $+Z$ direction and they are of equal strength, i.e., $\mathfrak{h}_n = \mathfrak{h}\,\forall\, n$. We choose $\mathfrak{h} = 0.5$. All the helices are taken as right-handed and the results are performed considering $N = 30$.

In computing the results, we set the "high-frequency regime" for the incident light irradiation. This is an important and realistic approximation, and it is defined by the condition $\hbar\omega \gg 4t_1$. Most of the studies available in the literature involving electron and spin-dependent transport phenomena essentially focused on the high-frequency regime, and here also we follow it. In this regime, the Floquet bands are uncoupled, and only the zeroth order Floquet band dominates, i.e., $p = q = 0$. The other higher order terms associated with p and q have vanishingly small contribution. Under this situation, the quasienergy of each Floquet band is identical to the energy bands of the undriven system with the renormalized hopping strength

$$\tilde{t}_{nj}^{p=0,q=0} = t_{nj}J_0(\Lambda)e^{-(l_{nj}-l_1)/l_c}.$$

The factor $J_0(\Lambda)$ contains all the information of light irradiation. As the hopping integrals are directly influenced by the light, the modification of transport behavior with light is naturally expected.

On the other hand, in the low-frequency regime, we need to consider the coupling of the parent magnetic helix with its several virtual copies, since the contributions from the higher order terms associated with p and q are not negligibly small. The concept of virtual copies along with the parent lattice comes from the fact that as per the Floquet formalism a $\mathcal{D}$-dimensional driven quantum system maps to a $(\mathcal{D}+1)$-dimensional undriven system (for a clear demonstration of it, see Ref. [47]). Once the several virtual copies are taken into account, two situations can happen. In one case, due to the large effective system size, the average energy level spacing will be small compared to the thermal energy, and in the other

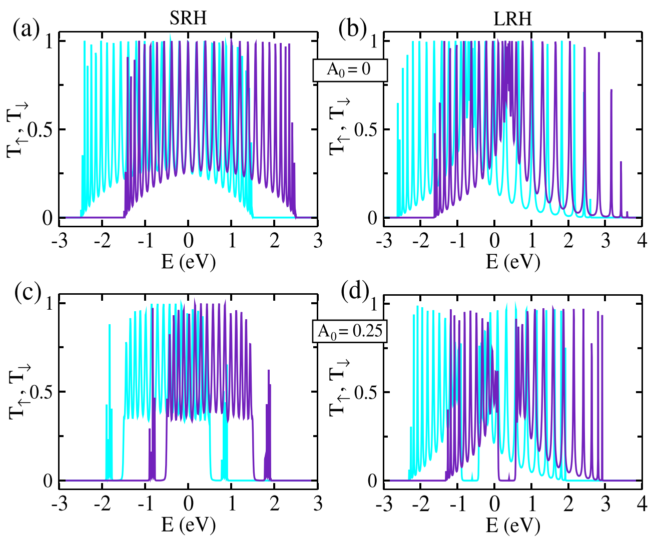

FIG. 2. Up (cyan) and down (indigo) spin transmission probabilities as a function of energy for the SRH (left column) and LRH (right column) magnetic helices in the absence ($A_0 = 0$) and presence ($A_0 = 0.25$) of light irradiation.

case, the effective system size becomes larger than the spin coherence length [61]. Because of these facts, the getting of favorable spin-dependent phenomena may be hindered.

The arguments presented above indicate that high-frequency limit is recommended to have a favorable response. In such a limit, the frequency of the incident light should be at least $\sim 10^{16}$ Hz, and it belongs to the ultraviolet (UV)/extreme UV regime. The intensity of the irradiation is $\sim 10^5$ W/m^2, and it is well within the experimental reach. Light of much higher intensities has already been taken into account in many other contemporary studies [62,63], and thus, our chosen intensity can safely be used and it will not damage the physical system.

Now we present and analyze our results one by one.

We begin with Fig. 2 which displays the spin-specific transmission probabilities as a function energy for the SRH and LRH magnetic helices in the full available energy window. In Fig. 3, we replot the transmission spectra of Fig. 2 in a small energy region which is well inside the band (reason of considering the energy zone well inside the full window is given later) for better viewing of up and down spin transmission profiles and to examine the interplay between the helicity and light irradiation more clearly. The results are worked out both in the absence and presence of light irradiation. Several important features are obtained those are as follows. First, in each subfigure of Fig. 2 (and also of Fig. 3), a finite mismatch is observed between the up and down spin transmission spectra. This is due to the spin-dependent scattering of itinerant electrons with the local magnetic

moments at different lattice sites of the helix. And, the large shifting of up spin transmission spectrum with respect to the other is due to the "strong" spin-dependent scattering strength $\mathfrak{h}$. It is important to mention here that such a mismatch cannot be obtained in other spin-dependent scattering processes as they are usually very small in strength [4]. Second, in the absence of light irradiation, the resonant

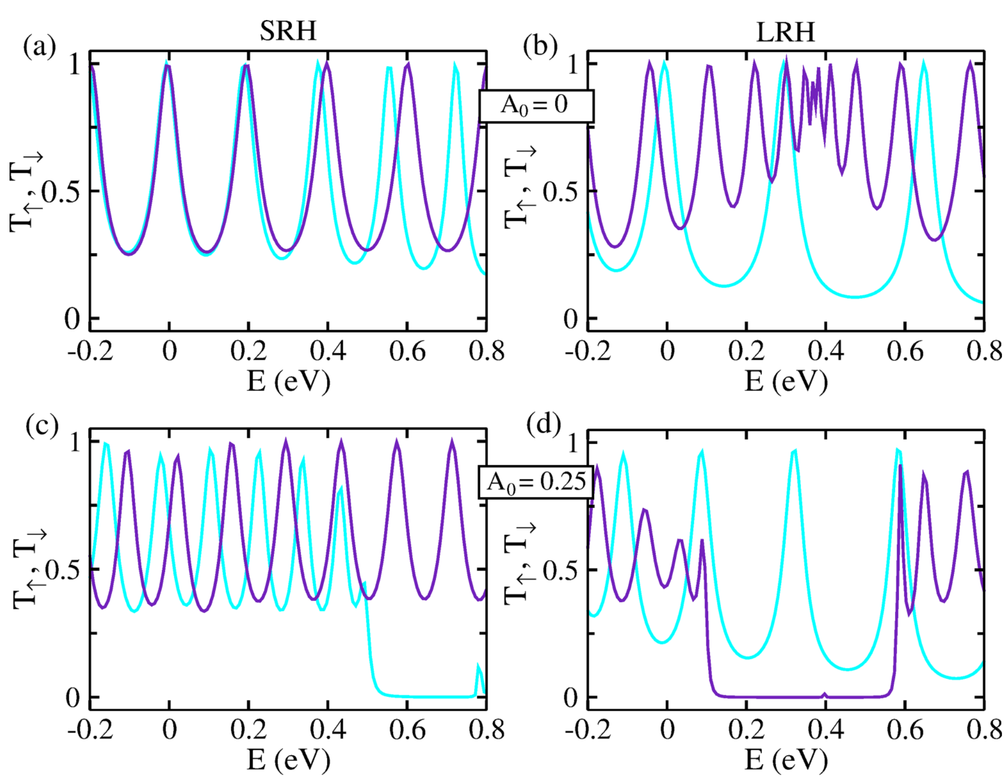

FIG. 3. Replot of different spectra of Fig. 2 in a small energy window for better viewing of transmission profiles and to see more clearly the interplay between the helicity and light irradiation. The colors of the transmission curves ($T_\uparrow \rightarrow$ cyan color, $T_\downarrow \rightarrow$ indigo color) and all the parameters are exactly identical as used in Fig. 2.

transmission peaks exhibit nearly uniform spacing in the case of SRH magnetic helix [Figs. 2(a) and 3(a)]. Conversely, for the LRH helix, the transmission peaks demonstrate nonuniform spacing. In the low-energy region, the peaks are closely clustered, whereas in the high energy region, the spacing between the peaks becomes more pronounced ([Fig. 2(b)]. The nonuniform spacing of the resonant transmission peaks occurs due to the breaking of the electron-hole symmetry in presence of higher order hopping. With increasing the range of electron hopping the successive gap between the resonant peaks enhances in the limit of high energies. Such nonuniform distribution of resonant peaks may lead to enhanced spin polarization in the LRH system, that can be understood form our forthcoming discussion. All these peaks are associated with the available energy eigenvalues of the magnetic helices, and thus, from the nature of transmission profile, the eigenspectrum of the helix can be estimated. Here it is worthy to note that, the uniform spacing throughout the energy window is available only for the nearest-neighbor hopping model (see Fig. 13 of Appendix B), and for this case electron-hole symmetry is no longer violated.

Third, the transmission spectrum gets modified once the helix is irradiated with light, and the effect becomes significant for the LRH system. The spacing between the successive transmission peaks is more nonuniform for the irradiated LRH helix than the irradiation-free case, which is clearly reflected by comparing the spectra given in the right column of Fig. 3. For the SRH helix, the effect of irradiation is not so prominent. As already mentioned, the nonuniform spacing of the resonant transmission peaks is solely due to the breaking of electron-hole symmetry in presence of higher order hopping. Now the origin of short-range or long-range hopping of electrons and the role of irradiation can be clearly understood by noting the hopping strengths between the first few neighboring sites of the helices, both in the absence and presence of irradiation. For the SRH helix, the first few hopping strengths in the absence of light are $1,\ 3.19 \times 10^{-3},\ 1.99 \times 10^{-5},\ 2.95 \times 10^{-7},\ 1.07 \times 10^{-8}$, and in the presence of light these are: $0.661,\ 2.97 \times 10^{-4},\ -8.035 \times 10^{-6},\ 8.41 \times 10^{-8},\ -1.52 \times 10^{-9}$. Whereas for the LRH helix, the first few hopping strengths in the absence and presence of lights are $1,\ 0.159439,\ 0.316866,\ 0.0942651,\ 0.0051797$ and $0.909652,\ 0.131288,\ 0.201565,\ 0.045867,\ 0.00150171$, respectively. From these data, it is seen that for the SRH helix, the hopping strength decreases sharply with increasing the distance, while for the LRH case, finite strength is available for far enough sites. The notable thing is that for the irradiated LRH system, the rate of change of hopping from the first neighbor hopping becomes less compared to the irradiation-free situation, and we confirm it for several other light parameters as well. It indicates that, in presence of light, the LRH effect becomes more prominent than the light-free condition, and accordingly, electron-hole symmetry breaking becomes more evident, resulting higher gaps between successive transmission peaks. Because of this, larger mismatch among up and down spin transmission profiles is obtained due to light [Fig. 3(d)], and high degree of spin polarization is favorable. The symmetry breaking in the SRH helix is relatively weak, even in the presence of light, as all the other hopping strengths compared to the first neighbor

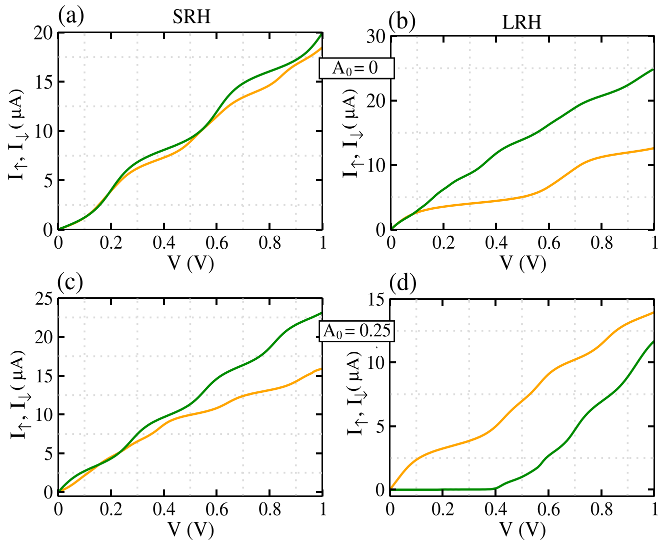

FIG. 4. Up (orange curve) and down (dark green curve) spin currents as a function of voltage for the SRH and LRH helices in the absence (first row) and presence (second row) of light irradiation. The currents are worked out for $E_F = 0.3$ eV.

are too small. In addition to the above facts, for the SRH helix, we find two distinct large gaps along the two edges of the transmission spectrum, whereas for the LRH helix one such large gap arises around the center of the spectrum. The appearance of these gaps is connected to the modification of energy eigenvalues of the magnetic helices in the presence of light. The key observation is that, when there is a gap in the transmission spectrum for (say) up spin electrons, the opposite spin electrons can fully transmit through that region, and vice versa. In such region(s), the 100% spin polarization is thus expected.

Once we get the transmission spectra for up and down spin electrons, then we can easily analyze the behavior of spin-dependent currents as a function of voltage bias. The results of spin-specific currents are given in Fig. 4. In determining junction current, we need to specify the Fermi energy E_F, and here we set $E_F = 0.3$ eV which is well inside the energy band. From the transmission spectra, displayed in Fig. 2, it is clear that if we set the Fermi energy around any of the two edges of the allowed energy window where only one type of spin electrons can transmit, we get finite current for that spin electrons and zero current for the other case, yielding a 100% spin polarization. However, experimentally it is too hard to set the Fermi energy at any of the two edges. On the other hand, fixing of E_F towards the center of the band is meaningful, and achieving the large degree of spin polarization under this situation is challenging. This is exactly our main focus of the present work. For our chosen E_F, we find that, the up and down spin currents are almost comparable to each other for the SRH helix when it is free from any irradiation [Fig. 4(a)]. This can be understood from the transmission-energy spectrum Fig. 3(a) which shows that within the chosen energy window ($E_F - eV/2 \leqslant E \leqslant E_F + eV/2$), both up and down spin electrons transmit, and hence the currents are almost comparable. In all the sub-figures of Fig. 3 such an energy range is selected for which the integration of the transmission curves is made to

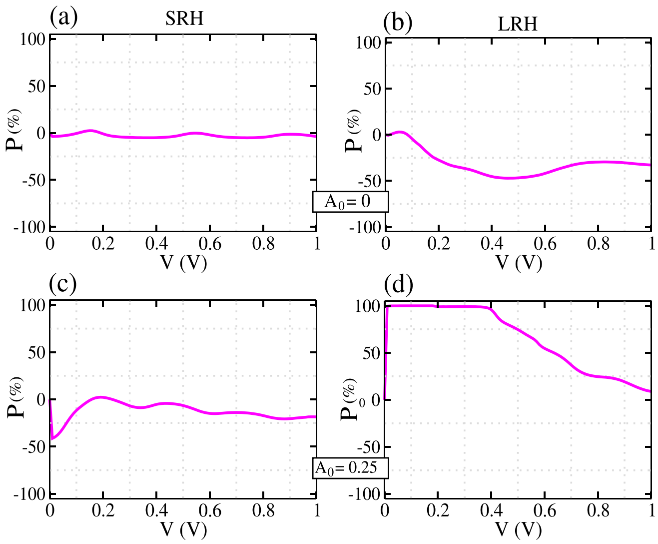

FIG. 5. Variation of spin polarization as a function bias voltage for the SRH and LRH helices under the irradiation free and with irradiation cases. The Fermi energy is same as mentioned in Fig. 4.

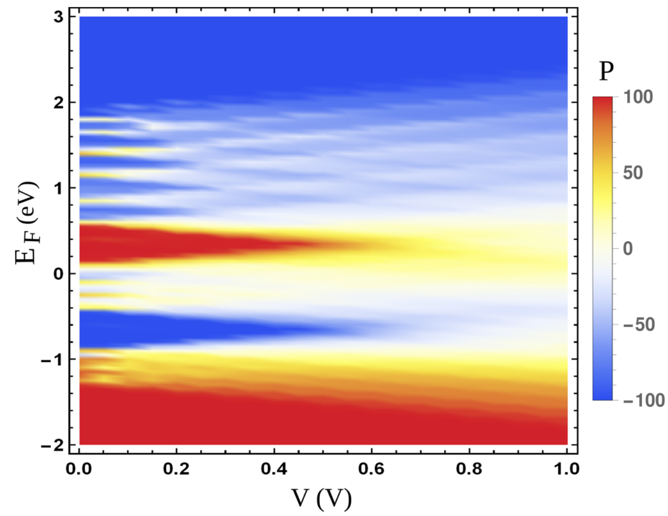

FIG. 6. Density plot. Simultaneous variation of spin polarization coefficient P with Fermi energy E_F and the bias voltage V for the LRH magnetic helix. Here we set $A_0 = 0.25$.

compute the spin-dependent currents presented in Fig. 4. The maximum chosen voltage $V = 1$ V corresponds to the energy range -0.2 eV to 0.8 eV. For the LRH helix, the currents are quite different [Fig. 4(b)]. This is due to finite mismatch of up and down spin transmission peaks within the above mentioned energy window [Fig. 3(b)]. The difference between the two currents increases once the light is injected to the system, and the effect becomes more prominent for the case of LRH helix, corroborating the transmission spectra given in Figs. 3(c) and 3(d), respectively. In the low bias region, while the up and down spin currents are quite comparable for the SRH helix [Fig. 4(c)], they are largely different for the LRH one [Fig. 4(d)]. Up to $V = 0.4$ V, down spin current is vanishingly small, while finite current is achieved for the other spin case [Fig. 4(d)]. Such a situation provides a high degree of spin polarization.

From the dependence of spin currents with bias voltage, it is now easy to follow the behavior of spin polarization. The nature of P-V curves is given in Fig. 5, where the Fermi energy and all other physical factors remain same as mentioned in Fig. 4. For the SRH magnetic helix, the response is too weak throughout the voltage window taken into consideration [Fig. 5(a)], reflecting the current-voltage curves plotted in Fig. 4(a). A slight improvement occurs in the presence of light irradiation [Fig. 5(b)]. The results for the LRH helix, on the other hand, are quite interesting. Even when $A_0 = 0$, more than 40% spin polarization is obtained [Fig. 5(c)], and it persists over a moderate bias window. However, the degree of spin polarization raises very close to 100% for a reasonable bias region when the helix is irradiated with light [Fig. 5(c)]. Thus the irradiation has a strong impact to improve the spin filtration. This improvement is solely due to the modification of up and down spin energy channels, and thus, the transmission spectra. The above analysis clearly suggests that in presence of spin-dependent scattering, the electron-hole symmetry breaking caused by the higher order hopping plays a central role to achieve a high degree of spin polarization, and the effect becomes more superior with the application of light as it enhances the symmetry breaking mechanism.

Since the transmission spectrum is directly influenced by the light parameter, and the choice of E_F is also quite crucial, it is pertinent to check the effects of all these factors on spin polarization by varying them in a wide range, for the sake of completeness of our analysis.

Figure 6 presents the simultaneous variation of spin polarization coefficient as functions of Fermi energy E_F and the bias voltage V. Here we take the LRH magnetic helix, and set the amplitude of light irradiation $A_0 = 0.25$. Interestingly we find that, there exists several parameter zones where the degree of spin polarization reaches almost to 100%. Moreover, a complete phase reversal of P (+100% to -100%, and vice versa) is also obtained upon changing the physical parameters. All these issues are associated to the availability of up and

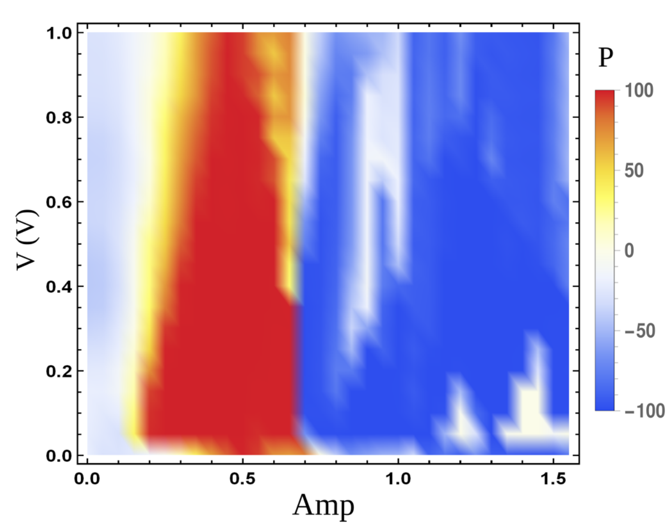

FIG. 7. Density plot. Simultaneous variation of P with A and V for the LRH magnetic helix. Here we choose $E_F = 0.25$ eV.

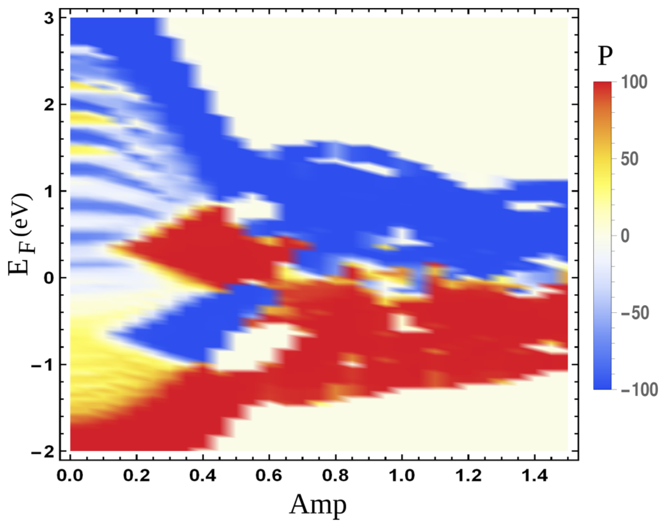

FIG. 8. Density plot. Simultaneous variation of P with E_F and A for the LRH case, when the bias voltage is fixed at 0.2 V.

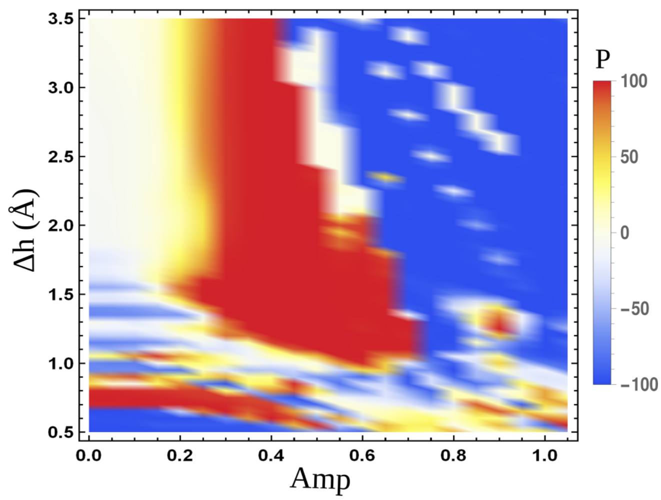

FIG. 9. Density plot. Simultaneous variation of P with Δh and A, with $E_F = 0.25$ eV and $V = 0.2$ V. For the helix system considered here, the other three physical parameters, $\Delta\phi$, R, and l_c are kept constant with the LRH helix.

down spin energy channels, and how one type of spin channel dominates the other.

Next, in Fig. 7, we show the dependence of P on the light amplitude A_0 and bias voltage V, when the Fermi energy is fixed. The results are really fascinating. For a wide range of A_0 and V we can have a very large value of P. And most importantly, the phase of spin polarization can be tuned selectively by monitoring the light amplitude. With the change of A_0, hopping integrals are modified, and accordingly, the up and down spin energy channels which gives the modification in P.

Figure 8 displays the dependence of P on A_0 and E_F, when the bias voltage is fixed. Like Figs. 6 and 7, here also we consider long-range hopping helix system. As expected, P can have +100% or −100%, depending on the choices of E_F and A_0. With increasing A_0, the hopping integrals get reduced, following the zeroth order Bessel function, and hence, the allowed energy window decreases. The energy band narrowing is reflected from this density plot.

In Fig. 9, we present a density plot where the variation of P is shown with respect to the light amplitude A_0 and the stacking distance Δh. The other three parameters of the helix viz, R, $\Delta\phi$, and l_c remain unchanged with the LRH helix given in Table I. The aim of this plot is to show how the response gets modified with the hopping strengths, as Δh is directly involved on these. It is clearly noticed from Fig. 9 that for a broad range of Δh, favorable spin polarization can be obtained, and selectively adjusting the light amplitude, we can have up or down spin polarization.

(1) *Role of helicity: dependence of spin polarization on* $\Delta\phi$. To explore the role of helicity in a more rigorous way, in this section, we discuss the dependence of spin polarization on twisting angle $\Delta\phi$ by varying it in a wide range, and, also compare the results with twist-free magnetic systems viz, when $\Delta\phi$ is exactly zero. From this analysis, the importance of helicity can be understood more clearly.

Let us start with the situation when the system is free from any helicity, i.e., $\Delta\phi = 0$. Under this condition, the helical magnetic systems transformed into the linear magnetic ones. For such linear systems, the results of spin-specific currents and the corresponding spin polarization coefficients, in presence of light irradiation, are shown in Fig. 10. Here we also set $E_F = 0.3$ eV, as earlier.

For the SRH magnetic system, the up and down spin currents are almost comparable to each other [Fig. 10(a)], reflecting the transmission curves given in Fig. 11(a), which yields very weak spin polarization for the entire bias window [Fig. 10(c)]. For the LRH case, whereas, the up and down spin currents are slightly different (Fig. 10(b)), associated with the transmission curves shown in Fig. 11(b), and hence a finite spin polarization appears [Fig. 10(d)], though it is very less

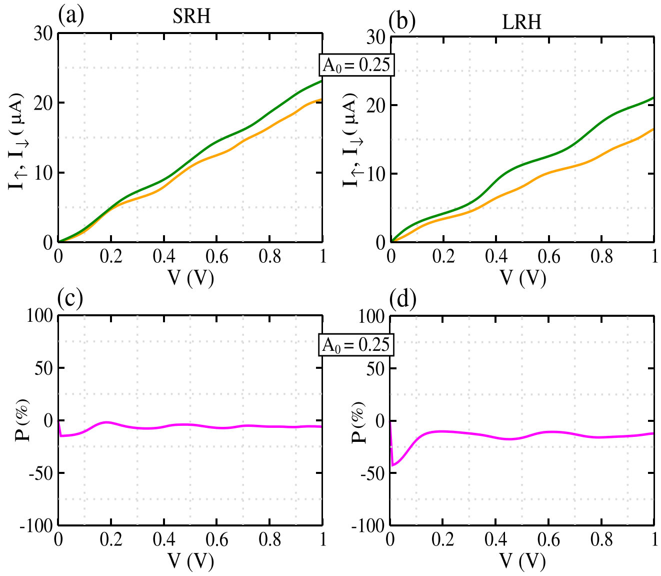

FIG. 10. Up (orange curve) and down (dark green curve) spin currents (first row) and variation of spin polarization (second row) as a function of voltage for the SRH and LRH magnetic systems in the absence of any helicity, i.e., when $\Delta\phi = 0$. Here we set $A_0 = 0.25$ and compute the currents for $E_F = 0.3$ eV.

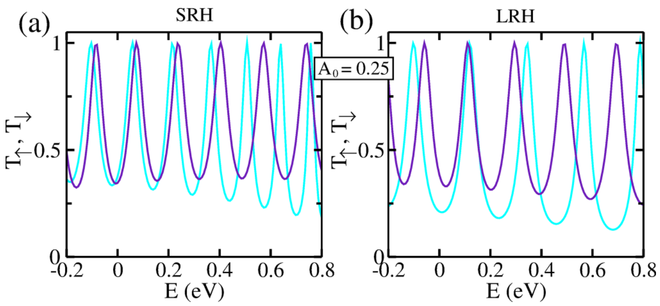

FIG. 11. $T_\uparrow$ (cyan) and $T_\downarrow$ (indigo) in a small energy window as selected in Fig. 3, for the physical systems with identical parameter values as considered in Fig. 10.

compared to the results discussed above for the magnetic systems in presence of finite helicity. When $\Delta\phi$ is set to zero, all the higher order hopping integrals are too small compared to the first-neighbor hopping. Thus the original LRH helix moves towards the NNH system, and the SSH helix goes more closer to the NNH one. Therefore much less electron-hole symmetry breaking effect is observed, resulting quite uniform spacing among the successive transmission peaks, as clearly noticed from the spectra given in Fig. 11. Because of this fact, the degree of spin polarization is reasonably small for the twist-less systems than the twisted ones. It clearly proves that helicity has a significant role as the factor Λ which is responsible to modulate the hopping integrals contains the components a_x^{nj}, a_y^{nj}, and a_z^{nj}, among which the first two components are directly involved with the twisting angle $\Delta\phi$ in a large extent (details are available in our theoretical formulation).

To have a direct impact of helicity and light on spin polarization, in Fig. 12, we present a density plot where the simultaneous variation of P is shown with respect to the twisting angle $\Delta\phi$ and the amplitude A_0. The interplay between A_0 and $\Delta\phi$ is really very interesting. When $\Delta\phi$ is zero and very small

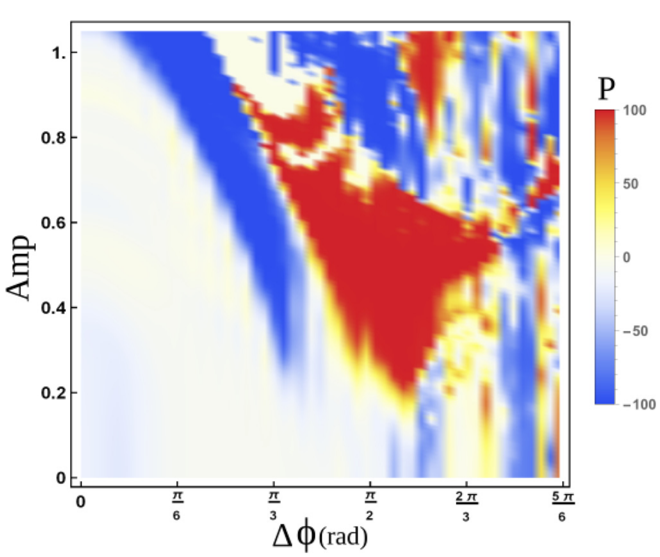

FIG. 12. Density plot. Simultaneous variation of P with $\Delta\phi$ and A, with $E_F = 0.25$ eV and $V = 0.2$ V. For the helix system considered here, the other three physical parameters, Δh, R, and l_c are kept constant with the LRH helix.

(close to zero), the degree of spin polarization is vanishingly small, corroborating the results discussed in Fig. 10. With increasing $\Delta\phi$, the blue colored region starts dominating for higher A_0 indicating -100% spin polarization, and a complete phase reversal takes place upon increasing the twisting angle. Around $\Delta\phi = 5\pi/9$, we get a very good response (almost $+100\%$ spin polarization) for a specific range of A_0. Thus the modification of Λ with the factors $\Delta\phi$ and A_0 is really important which is clearly reflected from our results.

(2) *Possible routes of achieving ferromagnetic helices*. A discussion about the possibilities of achieving ferromagnetic helices is indeed required for the sake of completeness of our analysis. Recent advances in experimental techniques have allowed us to design different kinds of magnetic helices. For instance, by electrodeposition and laser printing mechanism, Maurenbrecher *et al.* [64] have designed CoNi ferromagnetic helices. Quite a long ago, another researcher Ikuta has given a completely different prescription for generating helical magnetic configurations with the help of helical electromagnets [65]. In a work, Pati and his coworker have found helical magnetic configuration in vanadium-benzimidazole-modified sDNA sample [66], and they have shown that the system can exhibit half-metallic behavior in presence of the electric field. In 2016, Fust and coworkers have shown that topologically stabilized magnetic helices can be designed under suitable conditions and the magnetic ordering can persist even at large temperature limit [67]. Many other such references are available in the literature [68–73] which gives us confidence that our proposed magnetic helices can be substantiated in suitable laboratories.

IV. CLOSING REMARKS

In the present communication, we have investigated spin-dependent transport phenomena in magnetic helix systems, subjected to light irradiation. Two different kinds of helical systems have been taken into account, depending on the range of electron hopping. The central focus of the work is to explore the interplay between the helicity, different ranges of electron hopping and the light irradiation on spin selectivity. A tight-binding framework has been given to describe the Hamiltonian of the system, where the effect of light has been incorporated through Floquet-Bloch prescription within the minimal coupling scheme. The spin-specific transmission probabilities have been obtained following the well-known Green's function formalism, and the currents have been computed through the Landauer-Büttiker prescription. All the results have been carried out in the high-frequency limit, where the Floquet bands are decoupled and only the lowest order band contributes. For the benefit of the readers, a detailed mathematical description has been provided for the derivation of effective hopping in presence of light irradiation based on the FB method. Finally, we have given relevant experimental references where magnetic helices have been realized.

The key finding of our study are as follows. (i) A high degree of spin polarization can be obtained by adjusting the light amplitude. (ii) From 100% up spin polarization to 100% down spin polarization, and vice versa, can be made by means of light. (iii) All the results are valid for wide range of physical parameters which proves the robustness of our analysis.

The underlying mechanism of getting large response is solely associated with the breaking of electron-hole symmetry in presence of higher order hopping, and this effect becomes superior when the helix is subjected to light irradiation. With reducing the helicity the symmetry breaking effect gradually decreases, and in the limiting situation when $\Delta\phi = 0$, there is no electron-hole symmetry breaking for the system described with only nearest-neighbor hopping. Thus both the helicity and light irradiation are important.

Before an end, we would like to mention that the driven magnetic systems can be utilized as suitable functional elements for future spintronic applications. Similar kinds of other fascinating driven magnetic helices can also be taken into account to have several nontrivial signatures.

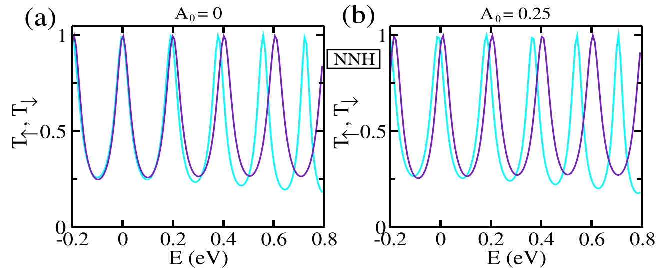

FIG. 13. $T_\uparrow$ (cyan) and $T_\downarrow$ (indigo) for a small energy window as selected in Fig. 3, for a ferromagnetic chain described with only NNH in the (a) absence and (b) presence of light.

APPENDIX A: FB THEORY: DETERMINATION OF EFFECTIVE HOPPING STRENGTH IN PRESENCE OF LIGHT IRRADIATION

Using the FB prescription, here we demonstrate the detailed mathematical steps to reach Eq. (6) that is mentioned in Sec. II A. We mostly adhere to the theoretical description given in Refs. [46,47], and the references therein. For any general Hamiltonian H (say) that is invariant under time and lattice translations viz, $H(\vec{x}+\vec{d}, \tau+\mathcal{T}) = H(\vec{x}+\vec{d}, \tau) = H(\vec{x}, \tau+\mathcal{T})$, the eigenfunctions can be expressed following the FB ansatz as

$$|\Psi_{\alpha,k}(\vec{x}, \tau)\rangle = e^{i\vec{k}\cdot\vec{x}} e^{-i\varepsilon_{\alpha,k}\tau/\hbar} |U_{\alpha,k}(\vec{x}, \tau)\rangle. \tag{A1}$$

Here $|U_{\alpha,k}(\vec{x}, \tau)\rangle$'s are the FB states those are periodic both in $\vec{x}$ and τ, $\vec{k}$ is the wave vector and $\varepsilon_{\alpha,k}$ denotes the quasienergy for the αth FB state. $|U_{\alpha,k}(\vec{x}, \tau)\rangle$ is associated to the composed Hilbert space (referred to as Sambe space) and it is formed by taking the direct product of the space related to time periodic function and the conventional Hilbert space.

To reach to Eq. (6), i.e., in order to determine the effective hopping in presence of irradiation, let us start with a general tight-binding Hamiltonian in the absence of any spin-dependent scattering (spin-dependent interaction does not have any effect in our forthcoming mathematical steps), for the sake of simplification. The prescription can then be utilized to any physical system. We choose the Hamiltonian as

$$H = \sum_{\alpha} \sum_{m,n} \gamma_{m,n} c^{\dagger}_{\alpha,m}(\tau) c_{\alpha,n}(\tau), \tag{A2}$$

where $c^{\dagger}_{\alpha,m}(\tau)$ and $c_{\alpha,m}(\tau)$ are the usual time-dependent creation and annihilation operators respectively, and $\gamma_{m,n}$ corresponds to the hopping strength between the lattice sites m and n. Defining the Fourier transform

$$c^{\dagger}_{\alpha,k}(\tau) = \sum_{m} c^{\dagger}_{\alpha,m}(\tau) e^{-i\vec{k}\cdot\vec{R}_m}, \tag{A3}$$

we express the operators as

$$c^{\dagger}_{\alpha,m}(\tau) = \sum_{k} c^{\dagger}_{\alpha,k}(\tau) e^{i\vec{k}\cdot\vec{R}_m} \tag{A4}$$

and

$$c_{\alpha,n}(\tau) = \sum_{k} c_{\alpha,k}(\tau) e^{-i\vec{k}\cdot\vec{R}_n}. \tag{A5}$$

Substituting these forms of the operators we get the Hamiltonian

$$H_k = \sum_{\alpha,k} \sum_{m,n} \gamma_{m,n} c^{\dagger}_{\alpha,k}(\tau) c_{\alpha,k}(\tau) e^{i\vec{k}\cdot(\vec{R}_m-\vec{R}_n)}. \tag{A6}$$

Due to time periodicity, we can expand the operators $c^{\dagger}_{\alpha,k}(\tau)$, $c_{\alpha,k}(\tau)$ in Fourier series as

$$c^{\dagger}_{\alpha,k}(\tau) = \sum_{p} c^{\dagger}_{\alpha k p} e^{-ip\omega\tau}, \tag{A7a}$$

$$c_{\alpha,k}(\tau) = \sum_{q} c_{\alpha k q} e^{iq\omega\tau}. \tag{A7b}$$

Plugging Eqs. (A7a) and (A7b) into Eq. (A6), we get

$$\begin{aligned} H_k &= \sum_{\alpha,k} \sum_{m,n} \sum_{p,q} \gamma_{m,n} e^{i\vec{k}\cdot(\vec{R}_m-\vec{R}_n)} e^{-i\omega\tau(p-q)} c^{\dagger}_{\alpha,k,p} c_{\alpha,k,q} \\ &= \sum_{\alpha,k} \sum_{m,n} \sum_{p,q} |U_{\alpha,k,p}\rangle \tilde{\gamma}_{m,n} e^{-i\omega\tau(p-q)} \langle U_{\alpha,k,q}|, \end{aligned} \tag{A8}$$

where

$$\tilde{\gamma}_{m,n} = \gamma_{m,n} e^{i\vec{k}\cdot(\vec{R}_m-\vec{R}_n)}.$$

Performing the composed scalar product, the quasienergies are calculated using H_k and mathematically expressed as

$$\begin{aligned} \varepsilon_{\alpha,k} &= \langle\langle U_{\alpha,k,p}|\mathscr{H}_k|U_{\alpha,k,q}\rangle\rangle \\ &= \frac{1}{\mathcal{T}} \int_0^{\mathcal{T}} \langle U_{\alpha,k,p}|\mathscr{H}_k|U_{\alpha,k,q}\rangle d\tau, \end{aligned} \tag{A9}$$

where $\mathscr{H}_k = H_k - i\hbar\frac{\partial}{\partial\tau}$. Following a long calculation, from Eq. (A9), we reach to the expression

$$\begin{aligned} \varepsilon_{\alpha,k} &= \sum_{m,n} \frac{1}{\mathcal{T}} \int_0^{\mathcal{T}} \gamma_{m,n} e^{i\vec{k}\cdot(\vec{R}_m-\vec{R}_n)} e^{-i\omega\tau(p-q)} d\tau + q\hbar\omega\delta_{p,q} \\ &= \sum_{m,n} \tilde{\gamma}^{p,q}_{m,n} + q\hbar\omega\delta_{p,q}, \end{aligned} \tag{A10}$$

where

$$\tilde{\gamma}^{p,q}_{m,n} = \frac{1}{\mathcal{T}} \int_0^{\mathcal{T}} \gamma_{m,n} e^{i\vec{k}\cdot(\vec{R}_m-\vec{R}_n)} e^{-i\omega\tau(p-q)} d\tau. \tag{A11}$$

Thus eventually we get an effective time-independent Hamiltonian [Eq. (A10)] with the site energy $q\hbar\delta_{p,q}$ and hopping strength $\tilde{\gamma}_{m,n}^{p,q}$. Applying the condition of the minimal coupling scheme [46,47], the effective hopping boils down to

$$\tilde{\gamma}_{m,n}^{p,q} = \frac{1}{\mathcal{T}} \int_0^{\mathcal{T}} \gamma_{m,n} e^{i\vec{A}\cdot(\vec{R}_m - \vec{R}_n)} e^{-i\omega\tau(p-q)} d\tau. \tag{A12}$$

Equation (A12) can now easily be generalized for our chosen helical systems. The hopping factor $\gamma_{m,n}$ will be replaced by $t_{nj}e^{-(l_{nj}-l_1)/l_c}$, $(\vec{R}_m - \vec{R}_n)$ will be changed to $(\vec{R}_{nj} - \vec{R}_n)$, and $\tilde{\gamma}_{m,n}^{p,q}$ will be replaced by $\tilde{t}_{nj}^{p,q}$. Thus the effective hopping of the helix in presence of light irradiation gets the form

$$\tilde{t}_{nj}^{p,q} = t_{nj} \frac{1}{\mathcal{T}} \int_0^{\mathcal{T}} e^{-i\omega\tau(p-q)} e^{i\vec{A}\cdot(\vec{R}_{nj} - \vec{R}_n)} d\tau e^{-(l_{nj}-l_1)/l_c}, \tag{A13}$$

which is exactly mentioned in Eq. (6).

APPENDIX B: TRANSMISSION SPECTRA OF A FERROMAGNETIC CHAIN DESCRIBED WITH NNH

For a 1D ferromagnetic chain described with only nearest-neighbor hopping, the hopping strength t_1 (say) gets modified due to light in a very simple form which reads as $t_1 J_0(A_0 l_1)$ (l_1 being the lattice spacing). Thus a 1D chain with nearest-neighbor hopping remains 1D with renormalized nearest-neighbor hopping in the presence of light, and hence, the electron-hole symmetry still persists. Therefore, both in the absence and presence of light, the spacing between the neighboring transmission peaks is uniform, as reflected from the spectra shown in Fig. 13. As the mismatch between the two spin-dependent transmission curves is too small, the degree of spin polarization will be very less.

[1] P. Zhang, Q. K. Xue, and X. C. Xie, Phys. Rev. Lett. **91**, 196602 (2003).
[2] W. Long, Q. F. Sun, H. Guo, and J. Wang, Appl. Phys. Lett. **83**, 1397 (2003).
[3] G. V. Lashkarev, M. V. Radchenko, M. E. Bugaiova, A. I. Dmitriev, V. I. Lazorenko, V. I. Sichkovskyi, W. Knoff, T. Story, Y. A. Stelmakh, and L. A. Krushynskaya, Low Temp. Phys. **39**, 66 (2013).
[4] Y. H. Su, S. H. Chen, C. D. Hu, and C.-R. Chang, J. Phys. D: Appl. Phys. **49**, 015305 (2016).
[5] E. I. Rashba, Phys. Rev. B **62**, R16267 (2000).
[6] N. Yamashita, E. Shigematsu, S. Honda, R. Ohshima, M. Shiraishi, and Y. Ando, Phys. Rev. Mater. **6**, 104405 (2022).
[7] G. Dresselhaus, Phys. Rev. **100**, 580 (1955).
[8] Y. A. Bychkov and E. I. Rashba, JETP Lett. **39**, 78 (1984).
[9] J. Chakraborty and N. Ganguli, Phys. Rev. B **102**, 214425 (2020).
[10] A. Machon, H.-C. Koo, J. Nitta, S. M. Frolov, and R. A. Duine, Nat. Mater. **14**, 871 (2015).
[11] R. Hanson and D. D. Awschalom, Nature (London) **453**, 1043 (2008).
[12] M. Johnson and R. H. Silsbee, Phys. Rev. Lett. **55**, 1790 (1985).
[13] D. Oue and M. Matsuo, Phys. Rev. B **102**, 125431 (2020).
[14] B. R. Bulka and S. Lipinski, Phys. Rev. B **67**, 024404 (2003).
[15] S. A. Wolf, D. D. Awschalom, R. A. Buhrman, J. M. Daughton, S. Von Molnár, M. L. Roukes, A. Y. Chtchelkanova, and D. M. Treger, Science **294**, 1488 (2001).
[16] I. Zutić, J. Fabian, and S. Das Sarma, Rev. Mod. Phys. **76**, 323 (2004).
[17] M. N. Baibich, J. M. Broto, A. Fert, F. Nguyen Van Dau, F. Petroff, P. Etienne, G. Creuzet, A. Friederich, and J. Chazelas, Phys. Rev. Lett. **61**, 2472 (1988).
[18] J. P. Lu, J. B. Yau, S. P. Shukla, M. Shayegan, L. Wissinger, U. Rössler, and R. Winkler, Phys. Rev. Lett. **81**, 1282 (1998).
[19] D. E. Nikonov, G. I. Bourianoff, and P. A. Gargini, J. Supercond. Novel Magn. **19**, 497 (2007).
[20] B. Göhler, V. Hamelbeck, T. Z. Markus, M. Kettner, G. F. Hanne, Z. Vager, R. Naaman, and H. Zacharias, Science **331**, 894 (2011).
[21] R. Gutiérrez, E. Díaz, R. Naaman, and G. Cuniberti, Phys. Rev. B **85**, 081404(R) (2012).
[22] Z. Xie, T. Z. Markus, S. R. Cohen, Z. Vager, R. Gutierrez, and R. Naaman, Nano Lett. **11**, 4652 (2011).
[23] K. Senthil Kumar, N. Kantor-Uriel, S. P. Mathew, R. Guliamov, and R. Naaman, Phys. Chem. Chem. Phys. **15**, 18357 (2013).
[24] Y. Wolf, Y. Liu, J. Xiao, N. Park, and B. Yan, ACS Nano **16**, 18601 (2022).
[25] R. Naaman and D. H. Waldeck, J. Phys. Chem. Lett. **3**, 2178 (2012).
[26] E. Medina, F. López, M. A. Ratner, and V. Mujica, Europhys. Lett. **99**, 17006 (2012).
[27] R. Otsuto, Y. Yatabe, and H. Akera, Phys. Rev. B **104**, 035431 (2021).
[28] S. Sarkar and S. K. Maiti, Phys. Rev. B **100**, 205402 (2019).
[29] Y. Zhang, J. He, and W.-J. Gong, Chem. Phys. Lett. **731**, 136596 (2019).
[30] S. Sarkar and S. K. Maiti, J. Phys.: Condens. Matter **34**, 455304 (2022).
[31] A.-M. Guo and Q.-F. Sun, Phys. Rev. Lett. **108**, 218102 (2012).
[32] A.-M. Guo and Q.-F. Sun, Proc. Natl. Acad. Sci. USA **111**, 11658 (2014).
[33] T.-R. Pan, A.-M. Guo, and Q.-F. Sun, Phys. Rev. B **92**, 115418 (2015).
[34] L. Deng, I. H. Bhat, and A.-M. Guo, J. Chem. Phys. **158**, 244116 (2023).
[35] G.-H. Liang, Y.-L. Wang, H. Jiang, M.-Y. Lai, and H.-S. Zong, J. Phys.: Condens. Matter **29**, 135801 (2017).
[36] Q. F. Sun and X. C. Xie, Phys. Rev. B **73**, 235301 (2006).
[37] T. P. Pareek, Phys. Rev. Lett. **92**, 076601 (2004).
[38] F. Chi, J. Zheng, and L. L. Sun, Appl. Phys. Lett. **92**, 172104 (2008).
[39] W. Gong, Y. Zheng, and T. Lü, Appl. Phys. Lett. **92**, 042104 (2008).
[40] Q. F. Sun and X. C. Xie, Phys. Rev. B **71**, 155321 (2005).
[41] A.-M. Guo and Q.-F. Sun, Phys. Rev. B **86**, 115441 (2012).
[42] F. Kuemmeth, S. Ilani, D. C. Ralph, and P. L. McEuen, Nature (London) **452**, 448 (2008).
[43] N. T. Phuc, J. Phys. Chem. Lett. **14**, 1626 (2023).

[44] N. T. Phuc, J. Chem. Phys. **159**, 054706 (2023).
[45] A.-M. Guo and Q.-F. Sun, Phys. Rev. B **95**, 155411 (2017).
[46] P. Delplace, Á Gómez-León, and G. Platero, Phys. Rev. B **88**, 245422 (2013).
[47] Á Gómez-León and G. Platero, Phys. Rev. Lett. **110**, 200403 (2013).
[48] S. Datta, *Electronic Transport in Mesoscopic Systems* (Cambridge University Press, Cambridge, 1997).
[49] S. Datta, *Quantum Transport: Atom to Transistor* (Cambridge University Press, Cambridge, 2005).
[50] M. D. Ventra, *Electrical Transport in Nanoscale Systems* (Cambridge University Press, Cambridge, 2008).
[51] D. S. Fisher and P. A. Lee, Phys. Rev. B **23**, 6851 (1981).
[52] G. Stefanucci, S. Kurth, A. Rubio, and E. K. U. Gross, Phys. Rev. B **77**, 075339 (2008).
[53] S. Kohler, J. Lehmann, and P. Hänggi, Phys. Rep. **406**, 379 (2005).
[54] S. Kurth, G. Stefanucci, C.-O. Almbladh, A. Rubio, and E. K. U. Gross, Phys. Rev. B **72**, 035308 (2005).
[55] G. Stefanucci and C.-O. Almbladh, Phys. Rev. B **69**, 195318 (2004).
[56] C. Verdozzi, G. Stefanucci, and C.-O. Almbladh, Phys. Rev. Lett. **97**, 046603 (2006).
[57] G. Stefanucci and C.-O. Almbladh, Europhys. Lett. **67**, 14 (2004).
[58] M. Patra and S. K. Maiti, Sci. Rep. **7**, 14313 (2017).
[59] D. Rai and M. Galperin, Phys. Rev. B **86**, 045420 (2012).
[60] R. G. Endres, D. L. Cox, and R. R. P. Singh, Rev. Mod. Phys. **76**, 195 (2004).
[61] A. E. Hansen, M. T. Björk, I. C. Fasth, C. Thelander, and L. Samuelson, Phys. Rev. B **71**, 205328 (2005).
[62] P. Karuppasamy, T. Kamalesh, K. Anitha, S. Abdul Kalam, M. S. Pandian, P. Ramasamy, Sunil Verma, and S. Venugopal Rao, Opt. Mater. **84**, 475 (2018).
[63] M. Murugesan, R. Paulraj, R. Perumalsamy, and M. K. Kumar, Appl. Phys. A **126**, 459 (2020).
[64] H. Maurenbrecher, J. Mendil, G. Chatzipirpiridis, M. Mattmann, S. Pané, B. J. Nelson, and P. Gambardella, Appl. Phys. Lett. **112**, 242401 (2018).
[65] K. Ikuta, Nucl. Fusion **23**, 75 (1983).
[66] S. S. Mallajosyula and S. K. Pati, J. Phys. Chem. B **111**, 13877 (2007).
[67] S. Fust, S. Mukherjee, N. Paul, J. Stahn, W. Kreuzpaintner, P. Böni, and A. Paul, Sci. Rep. **6**, 33986 (2016).
[68] L. V. Dzemiantsova, G. Meier, and R. Röhlsberger, Sci. Rep. **5**, 16153 (2015).
[69] N. Jiang, Y. Nii, H. Arisawa, E. Saitoh, J. Ohe, and Y. Onose, Phys. Rev. Lett. **126**, 177205 (2021).
[70] A. A. Povzner, A. G. Volkov, and I. A. Yasyulevich, Solid State Phenom. **257**, 30 (2016).
[71] E. J. Smith, D. Makarov, S. Sanchez, V. M. Fomin, and O. G. Schmidt, Phys. Rev. Lett. **107**, 097204 (2011).
[72] H. Wu and J. Lan, Phys. Rev. B **105**, 174427 (2022).
[73] O. M. Volkov, U. K. Röβler, J. Fassbender, and D. Makarov, J. Phys. D: Appl. Phys. **52**, 345001 (2019).